Dithiolenes Revisited: An Electron Spin Resonance Study of some Five-co-ordinate Cobalt Complexes and the Crystal Structures of $[Co\{S_2C_2(CF_3)_2\}_2\{P(OPh)_3\}]$ and $[Co\{S_2C_2(CF_3)_2\}_2(PPh_3)]$†

Gene B. Carpenter, Gregory S. Clark, Anne L. Rieger, Philip H. Rieger* and Dwight A. Sweigart
Department of Chemistry, Brown University, Providence, RI 02912, USA

Isotropic and frozen-solution ESR spectra in CH_2Cl_2–$ClCH_2CH_2Cl$ have been recorded for the five-co-ordinate, formally cobalt(IV) complexes $[Co(S_2C_2R_2)_2L]$ [R = CN, L = PEt_3; R = CF_3 or Ph, L = PPh_3 or $P(OPh)_3$; R = C_6H_4Me-4, L = PPh_3 or PEt_3; R = C_6H_4OMe-4, L = PPh_3]. The spectra can be described by approximately axial g and ^{59}Co hyperfine matrices with $g_{\|} = g_x \approx 1.99$, $g_{\perp} \approx 2.03$ and $A_{\|} = A_y \approx 61 \times 10^{-4}$ cm^{-1}, $A_{\perp} \approx 7 \times 10^{-4}$ cm^{-1}. These parameters are interpreted to show that the cobalt electronic structure is best regarded as low-spin d^5, formally Co^{IV}, but the singly occupied molecular orbital is extensively delocalized with only about 25% cobalt $3d_{xz}$ character. The g and A principal axes are displaced in the xy plane by the angle α which varies from 2 to 31°, increasing with the steric bulk of R and L. This angle is related to the degree of d_{xz}/d_{yz} hybridization resulting from molecular distortion from C_{2v} symmetry. The structures of $[Co\{S_2C_2(CF_3)_2\}_2L]$ [L = $P(OPh)_3$ or PPh_3] were determined by X-ray diffraction methods. Both complexes are approximately square pyramidal, but for L = $P(OPh)_3$ (diamagnetic in the solid state) the molecules are packed in the crystal as face-to-face pairs (Co···Co 4.11 Å). Extended-Hückel molecular-orbital calculations performed for $[Co\{S_2C_2(CF_3)_2\}_2\{P(OH)_3\}]$ support the interpretation of the ESR results.

1,2-Dithiolene complexes, which may be thought of as derived from anionic ethylene-1,2-dithiolates, $[S_2C_2R_2]^{2-}$, or from neutral 1,2-dithioketones, $S_2C_2R_2$, were the subject of many synthetic[1] and structural[2] studies in the 1960s and early 1970s. As might have been expected, given the ambiguity of the ligand oxidation state, most dithiolene complexes exhibit multiple oxidation states,[3] and much of the early work involved electrochemical studies. The variety of co-ordination geometries and oxidation states leads to mechanistic problems which attracted a variety of kinetic studies.[4] Many of the complexes are dimeric, *e.g.* $[\{Co[S_2C_2(CF_3)_2]_2\}_2]^{2-}$[2a] and $[\{Fe[S_2C_2(CN)_2]_2\}_2]^{2-}$,[2b] with two square-planar units bridged by metal–sulfur bonds, but these react with Lewis bases such as phosphines or phosphites to form mononuclear, presumably square-pyramidal, complexes, $[M(S_2C_2R_2)_2L]^{z-}$.[5]

Several ESR studies were reported for the five-co-ordinate cobalt complexes, $[Co(S_2C_2R_2)_2L]$ where the metal may be thought of as in oxidation state IV, and our interest in these complexes began with the preparation of a review of ESR studies of low-spin d^5 systems.[6] Although McCleverty and co-workers[5c] reported isotropic ESR spectra of a considerable number of anionic iron and neutral cobalt complexes, there was very little work on anisotropic spectra. Balch[5d] reported ESR parameters for $[Co\{S_2C_2(CF_3)_2\}_2L]$ [L = PPh_3, $P(OPh)_3$, $AsPh_3$ or $SbPh_3$] and Genser[7] published the spectrum of 0.2% $[Co(S_2C_2Ph_2)_2\{P(OPh)_3\}]$ doped in the isomorphous iron complex. After an extensive discussion he concluded that the singly occupied molecular orbital (SOMO) has Co $3d_{xy}$ character and that the complex is best regarded as containing Co^{II} with formally monoanionic ligands. Although Genser's spectrum is very well resolved, even a casual inspection shows that the apparent parallel features are not evenly spaced, a phenomenon which we have come to recognize as indicative of non-coincident g and hyperfine matrix principal axes.[8] Such non-coincident principal axes show the complex to have a symmetry lower than C_{2v}. We then undertook a reinvestigation of these complexes with several questions in mind: (1) is the structure really square pyramidal?; (2) if so, why do the ESR interaction matrices have non-coincident principal axes?; (3) what is the nature of the SOMO? and (4) from the perspective of the SOMO, what formal cobalt oxidation number, 4, 2, or even 0, is most appropriate?

In this paper we report isotropic and frozen-solution ESR spectra of eight five-co-ordinate cobalt complexes, $[Co(S_2C_2R_2)_2L]$ [R = CN, L = PEt_3; R = CF_3, L = PPh_3 or $P(OPh)_3$; R = Ph, L = PPh_3 or $P(OPh)_3$; R = C_6H_4Me-4, L = PPh_3 or PEt_3; R = C_6H_4OMe-4, L = PPh_3], the crystal structures of $[Co\{S_2C_2(CF_3)_2\}_2\{P(OPh)_3\}]$ and $[Co\{S_2C_2(CF_3)_2\}_2(PPh_3)]$ and extended-Hückel molecular orbital (EHMO) calculations for $[Co\{S_2C_2(CF_3)_2\}_2\{P(OH)_3\}]$.

Experimental

Chemicals.—Chlorinated solvents were distilled from calcium hydride under nitrogen. Hydrocarbons were dried over sodium. Other solvents were used as supplied. Triphenylphosphine (Aldrich) was recrystallized from ethyl acetate–hexane and vacuum dried. Liquid phosphines and phosphites were used as freshly supplied.

The complex $[\{Co[S_2C_2(CF_3)_2]_2\}_2]$ was prepared from $[Co_2(CO)_8]$ (Pressure Chemical Co.) and bis(trifluoromethyl)-1,2-dithietene by the method of Davison *et al.*[3b] The dithietane was prepared according to the method of Krespan.[9] The phosphine and phosphite derivatives were prepared by the method of Balch.[5d] The complexes $[\{Co(S_2C_2R_2)_2\}_2]$ (R = Ph, C_6H_4Me-4 or C_6H_4OMe-4) were synthesized using the method of Schrauzer *et al.*[5b] from the appropriate benzoin (Aldrich), phosphorus pentasulfide (Fisher) and cobalt(II) chloride (Baker). We found that using dioxane as solvent rather

† *Supplementary data available:* see Instructions for Authors, *J. Chem. Soc., Dalton Trans.*, 1994, Issue 1, pp. xxiii–xxviii.

Non-SI units employed: G = 10^{-4} T, eV ≈ 1.60×10^{-19} J.

than xylene gave much better yields of the 'thioester' intermediate in this synthesis. The phosphine or phosphite derivatives were prepared by the method of Schrauzer *et al.*[5b] Samples of the stable neutral compounds for ESR were prepared under argon in degassed CH_2Cl_2–$ClCH_2CH_2Cl$ (1 : 1).

The bis(maleonitriledithiolate) complex, $[NBu_4][Co\{S_2C_2(CN)_2\}_2]$ was prepared from $Na_2(mnt)$ (H_2mnt = 2,3-disulfanylmaleonitrile) and $CoCl_2$ according to the method of Davison and Holm.[1a] The PPh_3 and PEt_3 derivatives were prepared following the method of Gray and co-workers.[10] Neutral mnt complexes have not been reported. Electrochemical oxidation of $[Co\{S_2C_2(CN)_2\}_2L]^-$ failed to give observable ESR spectra. However, oxidation of the salt in CH_2Cl_2–$ClCH_2CH_2Cl$ with a less-than-stoichiometric amount of *p*-nitrobenzenediazonium tetrafluoroborate gave solutions which exhibited spectra. The L = PPh_3 complex was too short-lived to record spectra with good signal-to-noise ratio, but satisfactory results were obtained with the PEt_3 derivative.

The identity of all isolated compounds was checked by comparison of IR spectra with literature values and by mass spectrometric analysis.

Spectroscopy.—The ESR spectra were obtained with a Bruker ER-220D X-band spectrometer, equipped with a Bruker variable-temperature accessory or a liquid-nitrogen Dewar insert, a Bruker gaussmeter, a Systron-Donner microwave frequency counter, and an ASPECT-2000 computer. The IR spectra were obtained with a Mattson FT-IR spectrometer. Mass spectra were obtained with a Kratos MS80RFA spectrometer in positive-ion mode with fast atom bombardment using *m*-nitrobenzyl alcohol as a matrix.

X-Ray Crystallography.—Crystals of $[Co\{S_2C_2(CF_3)_2\}_2\{P(OPh)_3\}]$ and $[Co\{S_2C_2(CF_3)_2\}_2(PPh_3)]$ were grown from pentane by slow evaporation at −10 °C. X-Ray analyses were carried out using a Siemens P4 single-crystal diffractometer controlled by XSCANS software. Omega scans were used for data collection. Data reduction included profile fitting and an empirical absorption correction based on separate azimuthal scans for seven reflections (maximum and minimum transmission 0.644 and 0.577 for the phosphite structure, 0.850 and 0.724 for the phosphine structure). The first structure was determined by Patterson methods, the second by direct methods; both were refined initially by use of programs in the SHELXTL 5.1 package,[11] which were also used for all figures. Final refinements on F^2 were carried out using SHELXL 93.[12] Other details of the structure analyses are given in Table 7. Atomic coordinates are given in Tables 5 and 6 and selected bond lengths and angles in Tables 3 and 4. The molecular structures are shown in Figs. 4 and 5 and the unit-cell packing in Figs. 6 and 7.

Additional material available from the Cambridge Crystallographic Data Centre comprises H-atom coordinates, thermal parameters and remaining bond lengths and angles.

Results and Discussion

ESR Spectra.—The ESR spectra were obtained at room temperature and at 77 or 110 K for the eight dithiolene complexes, $[Co(S_2C_2R_2)_2L]$; data are listed in Table 1. The room-temperature spectra showed the expected ^{59}Co ($I = \frac{7}{2}$) octet; the spectra of the $P(OPh)_3$ complexes showed partial resolution of the ^{31}P coupling (a^P = 8.4 G) on the central lines of the octet.

The frozen-solution spectrum of $[Co\{S_2C_2(CF_3)_2\}_2\{P(OPh)_3\}]$ is shown in Fig. 1, together with a computer-simulated spectrum based on parameters described below. In general, the spectra show six or seven well resolved 'parallel' features and two or more 'perpendicular' features which are overlapped by the central parallel features. However, careful measurements showed that the parallel features are not evenly spaced, even after accounting for the small second-order shifts, a characteristic of a system with non-coincident *g* and hyperfine-matrix principal axes. For reasons discussed below, we label the parallel features *y* and assume that the non-coincidence effects are confined to the *xy* plane with the angle α between the *x* and *x'* axes. Assuming a small value of $A_{x'}$, the positions of the six (or seven) well resolved features can be fitted to give g_x, g_y, $A_{y'}$ and α. The remaining parameters, g_z and $A_\perp$ (assuming $A_{x'} \approx A_{z'}$), were then estimated from the isotropic parameters, $3\langle A\rangle = A_{x'} + A_{y'} + A_{z'}$, $3\langle g\rangle = g_x + g_y + g_z$. In all cases, $g_x \leqslant g_e$ and $g_y \approx g_z > g_e$ (g_e is the free-electron *g* value). Thus the spectra

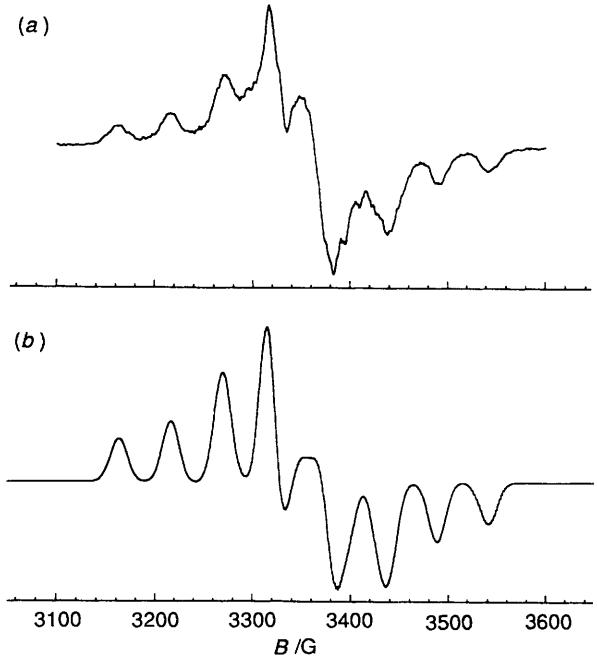

Fig. 1 (*a*) The ESR spectrum of $[Co\{S_2C_2(CF_3)_2\}_2\{P(OPh)_3\}]$ in CH_2Cl_2–$ClCH_2CH_2Cl$ at 77 K. (*b*) Computer simulation using the parameters of Table 1

Table 1 The ESR parameters

Complex	$\langle g\rangle$	$\langle A\rangle$[a]	g_x[b]	g_y[b]	$A_\parallel$[a,c]	α/°
$[Co\{S_2C_2(CN)_2\}_2(PEt_3)]$	2.025	26.2	2.001	2.040	67.9	2 ± 2
$[Co\{S_2C_2(CF_3)_2\}_2\{P(OPh)_3\}]$	2.015	24.8	1.996	2.020	59.1	11 ± 5
$[Co\{S_2C_2(CF_3)_2\}_2(PPh_3)]$	2.019	27.3	1.992	2.031	69.0	16 ± 1
$[Co(S_2C_2Ph_2)_2\{P(OPh)_3\}]$	2.010	22.0	1.990	2.025	50.6	11 ± 5
	(2.010[d])	(22.2[d])	(1.98[e])	(2.02[e])	(53[e])	(20 ± 2[e])
$[Co(S_2C_2Ph_2)_2(PPh_3)]$	2.010	25.3	1.984	2.026	61.1	24 ± 1
$[Co\{S_2C_2(C_6H_4Me\text{-}4)_2\}_2(PEt_3)]$	2.019	23.8	2.003	2.030	59.8	10 ± 2
$[Co\{S_2C_2(C_6H_4Me\text{-}4)_2\}_2(PPh_3)]$	2.012	24.6	1.984	2.027	60.8	24 ± 1
$[Co\{S_2C_2(C_6H_4OMe\text{-}4)_2\}_2(PPh_3)]$	2.013	26.2	1.984	2.032	59.1	31 ± 2

[a] $\times 10^4$ cm^{-1}. [b] ±0.001. [c] ±0.002. [d] From Genser.[7] [e] Reinterpretation of spectrum reported by Genser.[7]

can be understood semiquantitatively as arising from approximately axial g and ^{59}Co hyperfine matrices but with different parallel axes for the g matrix (x) and the hyperfine matrix (y'). The final fitted parameters are given in Table 1.

In most cases a few relatively sharp perpendicular features were resolved [or nearly so, see Fig. 1(*a*)]. With some effort, these would allow further refinement of g_z, $A_{x'}$ and $A_{z'}$, however the parameters of Table 1 reflect such a refinement only in the case of R = C_6H_4Me-4, L = PEt_3. A satisfactory computer simulation of the spectrum proved difficult in this case since the component widths appear to vary both with quantum number and orientation. In general, linewidths in the frozen-solution spectra were substantially greater than in the dilute crystalline powder spectrum reported by Genser[7] for $[Co(S_2C_2Ph_2)_2\{P(OPh)_3\}]$ and the ^{31}P hyperfine coupling was never resolved. For reasons discussed below, we have reinterpreted Genser's spectrum, with the results given in Table 1.

Interpretation of ESR Parameters.—We assume that these dithiolene complexes can be regarded, at least approximately, as either low-spin d^5, d^7 or d^9 systems, corresponding to formal oxidation states of +4, +2 or 0. If we define the Co–P bond as z and the bisectors of the S–Co–S bond angles as x and y, the erstwhile t_{2g} set of d orbitals is d_{xz}, d_{yz} and $d_{x^2-y^2}$. Assuming Co^{IV}, one of the t_{2g} orbitals is the dominant metal contribution to the SOMO, and the major axis of the dipolar hyperfine-interaction matrix should be y, x or z for d_{xz}, d_{yz} and $d_{x^2-y^2}$, respectively. Spin–orbit coupling of the SOMO with other MOs leads to departures of the g components from g_e. These interactions are summarized qualitatively in Fig. 2. If we assume that MOs with significant d_{xy} or d_{z^2} character are well separated from the SOMO and that their interactions can be neglected, we obtain $g_{\|} \approx g_e$, $g_{\perp} > g_e$ with the $g_{\|}$ axis corresponding to x if the SOMO has d_{xz} character. Similar results are obtained for d_{yz}, with the $g_{\|}$ axis corresponding to x and for $d_{x^2-y^2}$ with the $g_{\|}$ axis corresponding to z. Since we know that the $g_{\|}$ axis does not correspond to the $A_{\|}$ axis, we can rule out a $d_{x^2-y^2}$-based SOMO. In square-pyramidal geometry the choice of d_{xz} or d_{yz} is arbitrary and we choose the former.

If the formal oxidation state were Co^{II} or Co^0 the metal contribution to the SOMO would be either d_{xy} or d_{z^2}. In either case the $A_{\|}$ axis would be z. For a d_{z^2} contribution to the SOMO, the $g_{\|}$ axis would also be z, so that this option can be rejected. Since $A_{\perp}$ is small, $\langle A \rangle$ and $A_{\|}$ must have the same sign. Since the isotropic coupling probably arises through spin polarization $\langle A \rangle$ is probably negative, adding another argument against a d_{z^2} contribution to the SOMO. If the metal contribution to the SOMO were d_{xy} all three g components should be greater than g_e so that this option appears unlikely.

If the SOMO were purely metal d_{xz} the principal axes of the g and hyperfine matrices would necessarily be coincident. The fact that they are not suggests either a significant off-diagonal contribution to the g matrix from ligand-atom spin–orbit coupling[13] or a degree of metal d-orbital hybridization. We have been unable to construct a plausible model based on ligand-atom spin–orbit coupling, but the d-hybridization model gives a sensible result.

Suppose that the metal contribution is mostly d_{xz}, but with a small d_{yz} admixture: $|SOMO\rangle = c_1|xz\rangle + c_2|yz\rangle + \cdots$. The dipolar hyperfine-interaction matrix then is[8a] as in equation (1) where P is the dipolar coupling parameter for ^{59}Co.

$$A_d = \frac{2}{7}P \begin{pmatrix} c_1^2 - 2c_2^2 & 3c_1c_2 & 0 \\ 3c_1c_2 & c_2^2 - 2c_1^2 & 0 \\ 0 & 0 & c_1^2 + c_2^2 \end{pmatrix} \quad (1)$$

The matrix can be diagonalized by rotation about the x axis by the angle α_A [equation (2)] to give expression (3).

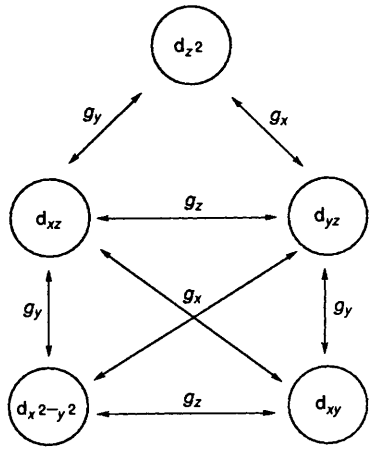

Fig. 2 Schematic representation of the spin–orbit coupling of d orbitals which results in contributions to the components of the g matrix

$$\tan 2\alpha_A = -\frac{2c_1c_2}{c_1^2 - c_2^2} \quad (2)$$

$$A_d = \frac{2}{7}P(c_1^2 + c_2^2) \begin{pmatrix} 1 & 0 & 0 \\ 0 & -2 & 0 \\ 0 & 0 & 1 \end{pmatrix} \quad (3)$$

Neglecting small contributions from spin–orbit coupling we have equation (4). With $P = 232 \times 10^{-4}$ cm^{-1},[14] we can use

$$A_{\|} - \langle A \rangle = -\frac{4}{7}P(c_1^2 + c_2^2) \quad (4)$$

the experimental parameters of Table 1 to compute the metal 3d spin densities listed in Table 2. The metal contribution to the SOMO is of the order of 25%, but with variations showing the influence of both the dithiolene substituent R and the axial ligand L.

If MOs with d_{z^2} and d_{xy} character are well removed from the SOMO so that spin–orbit coupling to these MOs can be neglected, the g-matrix components are[6] (5)–(8) where λ is the

$$g_{xx} = g_e + \frac{2\lambda c_2^2}{\Delta E_{x^2-y^2}} \quad (5)$$

$$g_{yy} = g_e + \frac{2\lambda c_1^2}{\Delta E_{x^2-y^2}} \quad (6)$$

$$g_{zz} = g_e + \frac{2\lambda c_1^2}{\Delta E_{yz}} + \frac{2\lambda c_2^2}{\Delta E_{xz}} \quad (7)$$

$$g_{xy} = \frac{2\lambda c_1 c_2}{\Delta E_{x^2-y^2}} \quad (8)$$

spin–orbit coupling parameter for cobalt and the ΔE terms are energy differences, averaged over MOs with energies E_k and LCAO (linear combination of atomic orbitals) coefficients c_{ik} [equation (9)]. The matrix is diagonalized

$$\frac{1}{\Delta E_i} = \sum_{k \neq 0} \frac{c_{ik}^2}{E_0 - E_k} \quad (9)$$

by rotation about the x axis by angle α_g [equation (10)] to give

$$\tan 2\alpha_g = \frac{2c_1c_2}{c_1^2 - c_2^2} \quad (10)$$

$g_X = g_e$ and g_Y as in equation (11). Since the rotations of the

Table 2 Cobalt contribution to SOMO

Complex	$c_1^2 + c_2^2$	c_2^2/c_1^2
$[Co\{S_2C_2(CN)_2\}_2(PEt_3)]$	0.31	0.0003 ± 0.0006
$[Co\{S_2C_2(CF_3)_2\}_2\{P(OPh)_3\}]$	0.26	0.009 ± 0.008
$[Co\{S_2C_2(CF_3)_2\}_2(PPh_3)]$	0.31	0.020 ± 0.003
$[Co(S_2C_2Ph_2)_2\{P(OPh)_3\}]$	0.22	0.009 ± 0.008
	(0.23)*	(0.031 ± 0.006)*
$[Co(S_2C_2Ph_2)_2(PPh_3)]$	0.27	0.045 ± 0.004
$[Co\{S_2C_2(C_6H_4Me\text{-}4)_2\}_2(PEt_3)]$	0.27	0.008 ± 0.003
$[Co\{S_2C_2(C_6H_4Me\text{-}4)_2\}_2(PPh_3)]$	0.27	0.045 ± 0.004
$[Co\{S_2C_2(C_6H_4OMe\text{-}4)_2\}_2(PEt_3)]$	0.25	0.077 ± 0.010

* From reinterpreted spectrum of Genser.[7]

$$g_Y = g_e + \frac{2\lambda(c_1^2 + c_2^2)}{\Delta E_{x^2-y^2}} \quad (11)$$

principal axes of the g and hyperfine matrices are equal and opposite, the observed angle can be written quite simply in terms of the hybridization ratio, $R = (c_2/c_1)^2$, *i.e.* as in equation (12).

$$\tan \alpha = -\frac{2\sqrt{R}}{1 - R} \quad (12)$$

As shown in Fig. 3, the angle α is an extremely sensitive measure of the hybridization ratio. Hybridization ratios computed from the observed angles are given in Table 2.

Structures of $[Co\{S_2C_2(CF_3)_2\}_2\{P(OPh)_3\}]$ *and* $[Co\{S_2C_2(CF_3)_2\}_2(PPh_3)]$.—As shown in Figs. 4 and 5, $[Co\{S_2C_2(CF_3)_2\}_2\{P(OPh)_3\}]$ and $[Co\{S_2C_2(CF_3)_2\}_2(PPh_3)]$ are approximately square pyramidal, although both structures show significant distortions from idealized C_{2v} symmetry. In the phosphite derivative S(1) is tilted out of the equatorial plane such that the complex could also be regarded as approximately trigonal pyramidal with S(1), S(3) and P equatorial, S(2) and S(4) axial. The distortion from square-pyramidal geometry can be ascribed to the non-bonded interaction of S(1) and the nearby phenyl ring of the $P(OPh)_3$ ligand; the shortest non-bonded distance is 3.33 Å between S(1) and the bridgehead carbon of the phenyl ring bonded to O(1). The phosphine complex is somewhat less distorted; in this case the distortion can be regarded as tilting of the phosphine ligand toward S(4).

As found in other dithiolene structures,[2] the C–C [1.363–1.370 and 1.346–1.369 Å for the $P(OPh)_3$ and PPh_3 complexes, respectively] and C–S (1.691–1.710 and 1.701–1.715 Å) bond lengths found in the dithiolene rings are reminiscent of those in sulfur heterocyclics such as thiophene [C(2)–C(3) 1.362, S–C(2) 1.712 Å].[15] This observation suggests that the metal dithiolene ring is best regarded as a six-electron π system with aromatic character. If, for the purposes of electron counting, all six π electrons are assigned to the ligand, we have Co^{IV} as a first approximation to the formal oxidation state of the metal.

The structures can be compared with those of $[Fe\{S_2C_2(CF_3)_2\}_2(AsPh_3)]$,[2d] $[Fe(S_2C_2Ph_2)_2\{P(OMe)_3\}]$[2e] and $[Fe(C_6H_4S_2)_2(PMe_3)]$.[16] None of these complexes has precise C_{2v} symmetry, but the $AsPh_3$ complex is much closer to the ideal than are the cobalt complexes. In the case of the $P(OMe)_3$ complex both S(1) and S(4) have non-bonded interactions with phosphite methoxyl groups (the atoms are numbered in analogy to Figs. 4 and 5); in the third complex the PMe_3 ligand is tilted significantly toward S(2) and S(3). Nonetheless, the equatorial planes are relatively symmetrical in the iron complexes; the ranges of *trans* S–Fe–S angles, for example, are 165.4–169.4, 161.2–162.8 and 167.4–168.2°, respectively, compared with 156.0–169.9 and 158.4–165.1° for the S–Co–S angles in the $P(OPh)_3$ and PPh_3 derivatives; similarly, the ranges of Fe–S bond lengths are 2.145–2.154, 2.152–2.177 and 2.183–2.187 Å compared with 2.143–2.172 and 2.155–2.164 Å for the Co–S lengths.

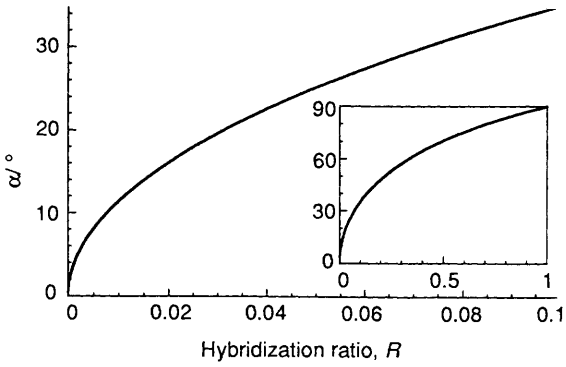

Fig. 3 Non-coincidence angle α as a function of the d_{yz}/d_{xz} hybridization ratio

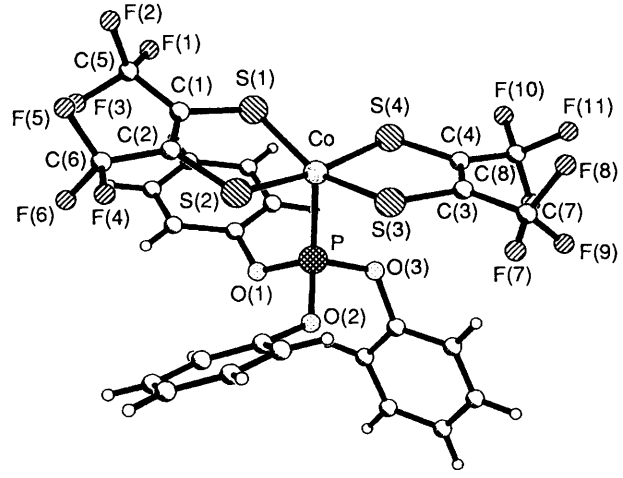

Fig. 4 The molecular structure of $[Co\{S_2C_2(CF_3)_2\}_2\{P(OPh)_3\}]$ showing the atom labelling scheme

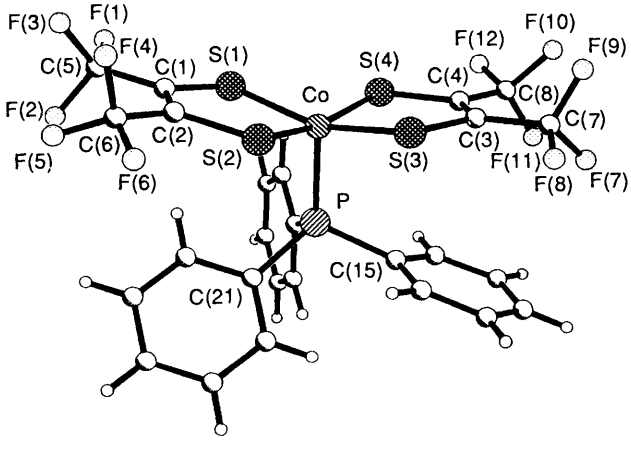

Fig. 5 The molecular structure of $[Co\{S_2C_2(CF_3)_2\}_2(PPh_3)]$ showing the atom labelling scheme

Perhaps the most interesting aspect of the structures is the packing of molecules in the unit cells. As shown in Fig. 6, $[Co\{S_2C_2(CF_3)_2\}_2\{P(OPh)_3\}]$ molecules are packed face-to-face with a Co · · · Co distance of 4.11 and 3.82 Å between S(2) and S(4A). The packing for $[Co\{S_2C_2(CF_3)_2\}_2(PPh_3)]$, shown in Fig. 7, is entirely different with independent, essentially non-interacting molecules. The packing of $[Fe\{S_2C_2(CF_3)_2\}_2(AsPh_3)]$ is also face-to-face, but with molecules displaced to produce an Fe–S square array (Scheme 1), similar to, but with much weaker interactions than, the dimeric species [{Co[S_2-

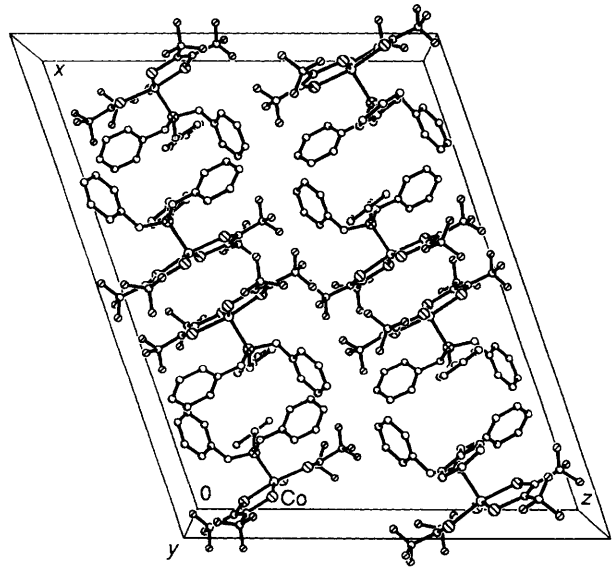

Fig. 6 Unit cell of $[Co\{S_2C_2(CF_3)_2\}_2\{P(OPh)_3\}]$, showing the face-to-face pairs of molecules. All hydrogen atoms have been omitted for clarity

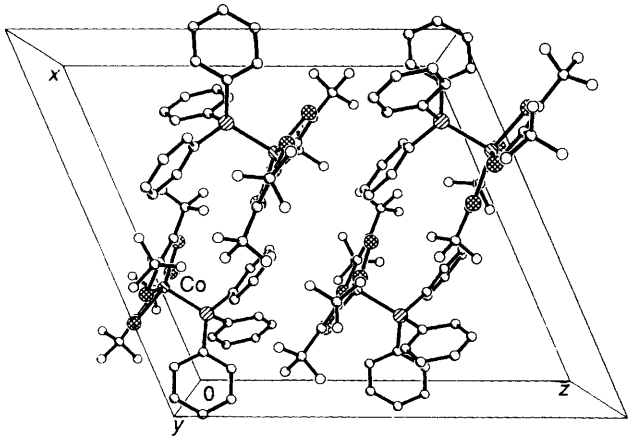

Fig. 7 Unit cell of $[Co\{S_2C_2(CF_3)_2\}_2(PPh_3)]$. All hydrogen atoms have been omitted for clarity

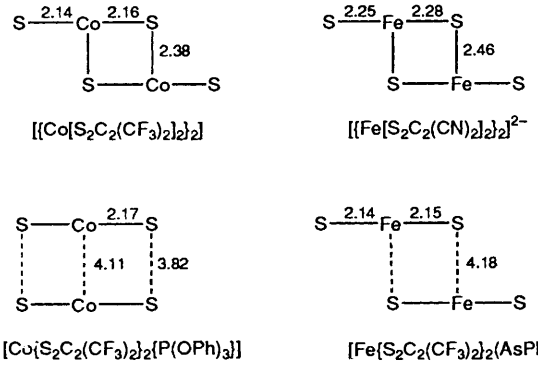

Scheme 1 Representation of the interaction (distances in Å) between monomer units in the dimeric species $[\{Co[S_2C_2(CF_3)_2]_2\}_2]$[1a] and $[\{Fe[S_2C_2(CN)_2]_2\}_2]^{2-}$[1b] and between mononuclear complexes in the unit cells of $[Co\{S_2C_2(CF_3)_2\}_2\{P(OPh)_3\}]$ and $[Fe\{S_2C_2(CF_3)_2\}_2(AsPh_3)]$[1c]

$C_2(CF_3)_2]_2\}_2]$[2a] and $[\{Fe[S_2C_2(CN)_2]_2\}_2]^{2-}$.[2b] The other iron complexes are packed quite differently: $[Fe(S_2C_2Ph_2)_2\{P(OMe)_3\}]$ molecules are in rather distant face-to-face pairs with a much larger displacement so that the shortest intermolecular Fe···S distance is over 10 Å; $[Fe(C_6H_4S_2)_2(PMe_3)]$ molecules are packed in a head-to-tail column.

Table 3 Selected bond lengths (Å) and angles (°) for $[Co\{S_2C_2(CF_3)_2\}_2\{P(OPh)_3\}]$

Co–P	2.123(1)	S(1)–C(1)	1.702(4)
Co–S(1)	2.143(1)	S(2)–C(2)	1.691(4)
Co–S(3)	2.150(1)	S(3)–C(3)	1.710(4)
Co–S(2)	2.171(1)	S(4)–C(4)	1.699(4)
Co–S(4)	2.172(1)	C(1)–C(2)	1.370(6)
P–O(3)	1.574(2)	C(1)–C(5)	1.514(6)
P–O(2)	1.578(3)	C(2)–C(6)	1.507(6)
P–O(1)	1.596(3)	C(3)–C(4)	1.363(5)
O(1)–C(9)	1.404(5)	C(3)–C(7)	1.507(6)
O(2)–C(15)	1.411(4)	C(4)–C(8)	1.514(6)
O(3)–C(21)	1.420(4)		
P–Co–S(1)	112.3(1)	C(3)–C(4)–S(4)	120.9(3)
P–Co–S(2)	94.39(5)	C(8)–C(4)–S(4)	115.1(4)
P–Co–S(3)	91.70(5)	C(1)–S(1)–Co	106.0(2)
P–Co–S(4)	95.68(4)	C(2)–S(2)–Co	104.8(2)
S(1)–Co–S(2)	89.84(4)	C(3)–S(3)–Co	104.5(2)
S(1)–Co–S(3)	156.0(1)	C(4)–S(4)–Co	103.6(2)
S(1)–Co–S(4)	86.25(5)	O(3)–P–Co	110.8(1)
S(2)–Co–S(3)	89.07(5)	O(2)–P–Co	120.6(1)
S(2)–Co–S(4)	169.9(1)	O(1)–P–Co	117.0(1)
S(3)–Co–S(4)	90.74(4)	O(3)–P–O(2)	99.61(14)
C(2)–C(1)–S(1)	118.7(3)	O(3)–P–O(1)	106.7(2)
C(5)–C(1)–S(1)	115.2(4)	O(2)–P–O(1)	100.0(2)
C(1)–C(2)–S(2)	120.5(3)	C(2)–C(1)–C(5)	126.1(4)
C(6)–C(2)–S(2)	115.9(4)	C(1)–C(2)–C(6)	123.4(4)
C(4)–C(3)–S(3)	119.4(3)	C(4)–C(3)–C(7)	126.5(4)
C(7)–C(3)–S(3)	114.1(4)	C(3)–C(4)–C(8)	123.8(4)

Table 4 Selected bond lengths (Å) and angles (°) for $[Co\{S_2C_2(CF_3)_2\}_2(PPh_3)]$

Co–S(2)	2.155(2)	S(2)–C(2)	1.704(5)
Co–S(3)	2.156(2)	S(3)–C(3)	1.707(6)
Co–S(4)	2.164(2)	S(4)–C(4)	1.715(6)
Co–S(1)	2.164(1)	C(1)–C(2)	1.369(7)
Co–P	2.219(1)	C(1)–C(5)	1.510(7)
P–C(15)	1.812(5)	C(2)–C(6)	1.497(7)
P–C(21)	1.823(5)	C(3)–C(4)	1.346(8)
P–C(9)	1.835(5)	C(3)–C(7)	1.516(8)
S(1)–C(1)	1.701(5)	C(4)–C(8)	1.523(8)
S(2)–Co–S(3)	84.17(6)	C(3)–C(4)–S(4)	119.7(4)
S(2)–Co–S(4)	165.1(1)	C(8)–C(4)–S(4)	113.8(5)
S(3)–Co–S(4)	89.33(6)	C(1)–S(1)–Co	105.4(2)
S(2)–Co–S(1)	89.55(5)	C(2)–S(2)–Co	106.1(2)
S(3)–Co–S(1)	158.4(1)	C(3)–S(3)–Co	105.5(2)
S(4)–Co–S(1)	91.67(6)	C(4)–S(4)–Co	104.9(2)
S(2)–Co–P	103.7(1)	C(15)–P–Co	109.7(2)
S(3)–Co–P	102.3(1)	C(21)–P–Co	113.5(2)
S(4)–Co–P	90.74(6)	C(9)–P–Co	118.9(2)
S(1)–Co–P	99.25(6)	C(15)–P–C(21)	108.7(2)
C(2)–C(1)–S(1)	120.0(4)	C(15)–P–C(9)	104.9(2)
C(5)–C(1)–S(1)	115.9(4)	C(21)–P–C(9)	100.4(2)
C(1)–C(2)–S(2)	118.8(4)	C(2)–C(1)–C(5)	124.0(5)
C(6)–C(2)–S(2)	114.9(4)	C(1)–C(2)–C(6)	126.3(5)
C(4)–C(3)–S(3)	119.5(4)	C(4)–C(3)–C(7)	125.7(6)
C(7)–C(3)–S(3)	114.7(5)	C(3)–C(4)–C(8)	126.5(6)

In his study of five-co-ordinate dithiolene complexes Balch[5d] reported that both $[Co\{S_2C_2(CF_3)_3\}_2\{P(OPh)_3\}]$ and $[Co\{S_2C_2(CF_3)_2\}_2(PPh_3)]$ are paramagnetic in solution and the latter is paramagnetic in the solid, but that the $P(OPh)_3$ derivative is diamagnetic in the solid state. We have confirmed the diamagnetism of the solid. Balch proposed a dimeric structure, analogous to that for $[Fe\{S_2C_2(CF_3)_2\}_2(AsPh_3)]$, but such a structure would make spin pairing even more surprising (the Fe···Fe distance is 4.79 Å). Indeed, Balch found that solid $[Co\{S_2C_2(CF_3)_2\}_2(AsPh_3)]$ is paramagnetic, so that if the iron and cobalt complexes are isostructural the molecules do not interact sufficiently strongly to induce spin pairing. The spacing in $[Co\{S_2C_2(CF_3)_2\}_2\{P(OPh)_3\}]$ is somewhat shorter and, with

a relatively large overlap area, analogous to that in a π complex, it may be possible to rationalize the observed spin pairing.

Extended-Hückel MO Calculations.—Extended-Hückel calculations were performed, using the default parameters supplied by the CAChe system,[17] for $[Co\{S_2C_2(CF_3)_2\}_2\{P(OH)_3\}]$ with atom coordinates based on the crystal structure of the $P(OPh)_3$ complex, taking the Co–P bond as the *z* axis and the average plane bisecting the S(1)–Co–S(2) and S(3)–Co–S(4) angles as the *xz* plane. Calculations were also performed on an idealized C_{2v} structure with the dithiolene-ring atom positions set to averages of the crystal structural positions. The metal 3d contributions to frontier and near-frontier orbitals are summarized in Table 8. There are several significant conclusions.

(1) The major metal contribution to the SOMO is d_{xz}, and MOs with major d_{z^2} and d_{xy} content are at least 1 eV above or below the SOMO energy; thus the conclusions reached in our ESR analysis and the assumptions made in the spin–orbit coupling calculations discussed above are at least qualitatively validated, *viz.* the electronic configuration can be regarded as a delocalized variation on the low-spin d^5 theme.

(2) In the C_{2v} structure the metal contribution to the SOMO is entirely d_{xz}, but in the distorted structure the SOMO has 28.5% metal d_{xz} character, 1.7% d_{yz} and smaller contributions from the other d orbitals, for a hybridization ratio as defined above, $R = 0.060$, again consistent with the assumptions made in the analysis presented above. It is probably significant, however, that the predicted hybridization ratio leads to a non-coincidence angle, $\alpha \approx 27°$, substantially greater than that observed for $[Co\{S_2C_2(CF_3)_2\}_2\{P(OPh)_3\}]$ in frozen solution. We will return to this point shortly.

(3) The computed metal 3d spin density is 0.32, in satisfactory agreement with the ESR result given in Table 2. The remaining spin density is delocalized on the dithiolene rings, but rather asymmetrically with the bulk of the spin on the S(3)–S(4) ring.

Table 5 Atomic coordinates (× 10^4) for $[Co\{S_2C_2(CF_3)_2\}_2\{P(OPh)_3\}]$

Atom	*x*	*y*	*z*	Atom	*x*	*y*	*z*
Co	656(1)	1059(1)	2279(1)	C(4)	−7(2)	2095(4)	995(2)
S(1)	594(1)	−910(1)	2464(1)	C(5)	877(2)	−2441(5)	3505(3)
S(2)	1001(1)	1390(1)	3296(1)	C(6)	1347(2)	−125(6)	4335(2)
S(3)	423(1)	3001(1)	2166(1)	C(7)	−72(2)	4474(6)	1165(3)
S(4)	194(1)	649(1)	1305(1)	C(8)	−257(2)	2126(6)	278(2)
P	1316(1)	1478(1)	2052(1)	C(9)	1662(2)	−885(4)	2120(2)
F(1)	734(2)	−3256(3)	3046(2)	C(10)	1373(2)	−1363(5)	1546(2)
F(2)	576(1)	−2554(3)	3856(2)	C(11)	1307(2)	−2662(5)	1485(2)
F(3)	1326(2)	−2760(3)	3883(2)	C(12)	1550(2)	−3438(5)	1993(2)
F(4)	1408(1)	1015(4)	4604(1)	C(13)	1846(2)	−2925(5)	2553(2)
F(5)	1135(1)	−800(3)	4671(1)	C(14)	1905(2)	−1643(4)	2628(2)
F(6)	1802(1)	−538(4)	4434(1)	C(15)	1872(2)	2966(4)	3000(2)
F(7)	139(2)	5308(3)	1598(2)	C(16)	2281(2)	2309(4)	3355(2)
F(8)	−557(1)	4616(3)	1056(2)	C(17)	2509(2)	2663(5)	3987(2)
F(9)	4(2)	4792(3)	643(2)	C(18)	2323(2)	3653(5)	4233(2)
F(10)	−414(1)	998(4)	45(1)	C(19)	1919(2)	4298(5)	3870(2)
F(11)	−670(1)	2822(4)	109(1)	C(20)	1689(2)	3972(4)	3242(2)
F(12)	32(1)	2547(4)	−24(1)	C(21)	1501(2)	2460(4)	1041(2)
O(1)	1741(1)	419(3)	2212(1)	C(22)	1939(2)	1972(5)	1027(2)
O(2)	1643(1)	2671(2)	2348(1)	C(23)	2222(2)	2674(6)	733(2)
O(3)	1186(1)	1793(3)	1320(1)	C(24)	2050(2)	3816(6)	458(2)
C(1)	868(2)	−1099(4)	3266(2)	C(25)	1606(2)	4262(5)	471(2)
C(2)	1052(1)	−58(4)	3633(2)	C(26)	1321(2)	3593(5)	766(2)
C(3)	90(2)	3144(4)	1372(2)				

Table 6 Atomic coordinates (× 10^4) for $[Co\{S_2C_2(CF_3)_2\}_2(PPh_3)]$

Atom	*x*	*y*	*z*	Atom	*x*	*y*	*z*
Co	3027(1)	1874(1)	268(1)	C(17)	3321(4)	4596(5)	2796(4)
S(1)	1894(1)	1434(1)	−955(1)	C(18)	4033(4)	4121(6)	3487(4)
S(2)	3445(1)	229(1)	485(1)	C(19)	4208(4)	3050(6)	3487(4)
S(3)	4438(1)	2183(1)	1178(1)	C(20)	3650(4)	2446(5)	2766(3)
S(4)	2877(1)	3538(1)	−97(1)	C(21)	1884(3)	880(4)	1475(3)
P	2227(1)	2118(1)	1108(1)	C(22)	1373(4)	156(5)	831(4)
C(1)	1957(4)	87(4)	−1018(3)	C(23)	1066(5)	−773(5)	1047(5)
C(2)	2654(3)	−461(4)	−375(3)	C(24)	1272(5)	−998(5)	1926(6)
C(3)	4554(4)	3534(5)	1207(4)	C(25)	1757(5)	−303(6)	2563(5)
C(4)	3859(4)	4136(4)	649(4)	C(26)	2071(4)	646(5)	2350(4)
C(5)	1187(4)	−433(5)	−1789(4)	F(1)	689(3)	255(3)	−2383(2)
C(6)	2810(5)	−1637(5)	−345(4)	F(2)	594(3)	−951(3)	−1554(3)
C(7)	5480(5)	3944(7)	1867(5)	F(3)	1494(3)	−1123(4)	−2213(3)
C(8)	3831(6)	5347(5)	606(4)	F(4)	3273(5)	−1906(4)	−810(5)
C(9)	1097(3)	2799(4)	637(3)	F(5)	2121(3)	−2211(3)	−584(5)
C(10)	688(4)	3185(4)	−225(3)	F(6)	3377(4)	−1968(3)	420(4)
C(11)	−190(4)	3651(5)	−513(4)	F(7)	5379(4)	4728(5)	2340(3)
C(12)	−651(4)	3726(5)	31(5)	F(8)	5922(4)	3257(5)	2449(4)
C(13)	−250(4)	3361(4)	874(4)	F(9)	5989(3)	4329(6)	1509(3)
C(14)	612(3)	2896(4)	1180(4)	F(10)	4582(4)	5742(4)	545(4)
C(15)	2913(3)	2897(4)	2071(3)	F(11)	3774(6)	5786(3)	1263(4)
C(16)	2743(4)	3979(4)	2089(3)	F(12)	3173(4)	5705(3)	−108(4)

Table 7 Crystal data and structure refinement*

	$[Co\{S_2C_2(CF_3)_2\}_2\{P(OPh)_3\}]$	$[Co\{S_2C_2(CF_3)_2\}_2(PPh_3)]$
Empirical formula	$C_{26}H_{15}CoF_{12}O_3PS_4$	$C_{26}H_{15}CoF_{12}PS_4$
M	821.52	773.52
Space group	$C2/c$	$P2_1/c$
a/Å	28.173(4)	15.603(2)
b/Å	10.5956(11)	12.5714(13)
c/Å	22.096(4)	16.454(2)
β/°	108.751(11)	113.138(7)
U/Å^3	6246(2)	2967.8(6)
Z	8	4
D_c/Mg m^{-3}	1.747	1.731
μ/mm^{-1}	0.970	1.007
$F(000)$	3272	1540
Crystal dimensions/mm	0.38 × 0.40 × 0.42	0.48 × 0.25 × 0.13
θ range for data collection/°	1.95–25.00	2.11–25.00
hkl ranges	−1 to 33, −1 to 12, −26 to 25	−1 to 18, −1 to 14, −19 to 18
Reflections collected	6481	6285
Independent reflections (R_{int})	5425 (0.0503)	5101 (0.0505)
Data, restraints, parameters	5425, 0, 424	5101, 0, 397
Goodness of fit on F^2	0.809	0.906
Final R indices [$I > 2\sigma(I)$]	$R1 = 0.0428$, $wR2 = 0.0817$	$R1 = 0.0537$, $wR2 = 0.1264$
R indices (all data)	$R1 = 0.0886$, $wR2 = 0.0907$	$R1 = 0.0926$, $wR2 = 0.1419$
Largest difference peak, hole/e Å^{-3}	0.344, −0.316	0.840, −0.446

* Details in common: T 298(2) K; λ(Mo-Kα) 0.710 73 Å; crystal system, monoclinic; full-matrix least-squares refinement on F^2; $w^{-1} = (\sigma F_o)^2 + (aP)^2$ where $P = [\max(F_o^2, 0) + 2F_c^2]/3$ and $a = 0.0277$, L = $P(OPh)_3$; a = 0.0760, L = PPh_3.

Table 8 Calculated metal d-orbital contributions to near-frontier MOs for $[Co\{S_2C_2(CF_3)_2\}_2\{P(OH)_3\}]$

	Idealized C_{2v} coordinates						X-Ray coordinates				
E/eV	z^2	xy	xz	yz	$x^2 - y^2$	E/eV	z^2	xy	xz	yz	$x^2 - y^2$
−5.900	—	—	—	—	—	−6.422	0.030	0.249	0.004	—	—
−6.297	—	0.312	—	—	—	−6.640	—	0.011	0.002	0.008	—
−6.699	0.213	—	—	—	—	−6.952	0.035	0.019	0.001	0.006	0.001
−8.372*	—	—	0.398	—	—	−8.358*	0.001	0.009	0.285	0.017	0.011
−8.867	—	—	—	0.828	—	−8.660	0.031	0.080	0.142	0.064	—
−8.919	—	—	—	—	0.968	−8.922	0.014	0.021	0.017	0.326	0.530
−9.253	—	—	0.316	—	—	−8.941	0.011	0.027	0.009	0.448	0.404
−9.332	0.650	—	—	—	—	−9.302	0.223	0.023	0.315	0.001	0.014
−9.471	—	—	—	0.129	—	−9.357	0.400	0.012	0.111	0.016	0.011
−9.493	0.001	—	0.277	—	—	−9.542	—	0.013	0.011	0.047	—
−9.732	—	0.638	—	—	—	−9.686	0.008	0.317	0.084	0.031	—

* Singly occupied molecular orbital.

Conclusion

Examination of the results summarized in Table 2 shows that there is an excellent correlation between the non-coincidence angle α and a qualitative expectation of steric crowding in $[Co(S_2C_2R_2)_2L]$. Thus α increases with R in the series CN < CF_3 < Ph ~ C_6H_4Me-4 < C_6H_4OMe-4 and with L in the series PEt_3 < $P(OPh)_3$ < PPh_3. Qualitative arguments then need not rely on the detailed line of causality involving hybridization ratios, and α may be taken simply as a sensitive measure of distortion from C_{2v} symmetry. With this insight we are in a position to propose explanations for several other puzzling observations.

The non-coincidence angle α found for the frozen-solution spectrum of $[Co\{S_2C_2(CF_3)_2\}_2\{P(OPh)_3\}]$ is significantly smaller than that for the spectrum of this complex doped into the diamagnetic iron analogue. It is also smaller than that predicted by EHMO calculations (based on the crystal structure). These observations suggest that the average distortion of the molecule in solution is rather less than that in the single crystal. Since the distortion in the crystal appears to be due to crystal packing, which forces a close contact of S(1) with one of the $P(OPh)_3$ phenyl rings, it is not surprising that other less-distorted conformations exist in solution.

Some components in frozen-solution spectra are significantly sharper than others, but all components are broader than in a dilute polycrystalline sample. The latter observation suggests that molecules in solution are subject to a variety of solvent interactions which lead to different molecular distortions and thus to different values of α (and probably slightly different g- and A-matrix components). Since this modulation affects different components in different ways, it is not surprising to find width variations within a spectrum and, on the average, greater widths than in a spectrum of dilute polycrystalline sample.

Acknowledgements

The X-ray equipment was purchased with assistance from an instrument grant from the National Science Foundation (CHE-8206423) and a grant from the National Institutes of Health (RR-06462). We are indebted to J. Van Epp for help with mass spectra, to R. Kershaw for determining magnetic susceptibilities, and to M. M. Banaszak Holl and A. Wold for stimulating discussions.

References

1 (*a*) A. Davison and R. H. Holm, *Inorg. Synth.*, 1967, **10**, 1; (*b*) J. A. McCleverty, *Prog. Inorg. Chem.*, 1968, **10**, 49.

2 (*a*) J. H. Enemark and W. N. Lipscomb, *Inorg. Chem.*, 1965, **4**, 1729; (*b*) W. C. Hamilton and I. Bernal, *Inorg. Chem.*, 1967, **6**, 2003; (*c*) E. F. Epstein, I. Bernal and A. L. Balch, *Chem. Commun.*, 1970, 136; (*d*) E. F. Epstein and I. Bernal, *Inorg. Chim. Acta*, 1977, **25**, 145; (*e*) H. Miyamae, S. Sata, Y. Saito, K. Sakai and M. Fukuyama, *Acta Crystallogr., Sect. B*, 1977, **33**, 3942.
3 (*a*) H. B. Gray, R. Williams, I. Bernal and E. Billig, *J. Am. Chem. Soc.*, 1962, **84**, 3596; H. B. Gray and E. Billig, *J. Am. Chem. Soc.*, 1963, **85**, 2019; (*b*) A. Davison, N. Edelstein, R. H. Holm and A. H. Maki, *J. Am. Chem. Soc.*, 1963, **85**, 2029; *Inorg. Chem.*, 1964, **3**, 814.
4 H. G. Tsiang and C. H. Langford, *Can. J. Chem.*, 1970, **48**, 2776; D. A. Sweigart, D. E. Cooper and J. M. Millican, *Inorg. Chem.*, 1974, **13**, 1272.
5 (*a*) R. Williams, E. Billig, J. H. Waters and H. B. Gray, *J. Am. Chem. Soc.*, 1966, **88**, 43; (*b*) G. N. Schrauzer, R. P. Mayweg, H. W. Finck and W. Heinrich, *J. Am. Chem. Soc.*, 1966, **88**, 4604; (*c*) N. G. Connelly, J. A. McCleverty and C. J. Winscom, *Nature* (*London*), 1967, **216**, 999; *J. Chem. Soc. A*, 1969, 2242; (*d*) A. L. Balch, *Inorg. Chem.*, 1967, **6**, 2158.
6 P. H. Rieger, *Coord. Chem. Rev.*, in the press.
7 E. E. Genser, *Inorg. Chem.*, 1968, **7**, 13.
8 (*a*) B. M. Peake, P. H. Rieger, B. H. Robinson and J. Simpson, *J. Am. Chem. Soc.*, 1980, **102**, 156; (*b*) B. M. Peake, P. H. Rieger, B. H. Robinson and J. Simpson, *Inorg. Chem.*, 1981, **20**, 2540; (*c*) W. E. Geiger, P. H. Rieger, B. Tulyathan and M. D. Rauch, *J. Am. Chem. Soc.*, 1984, **106**, 7000; (*d*) R. D. Pike, A. L. Rieger and P. H. Rieger, *J. Chem. Soc., Faraday Trans. 1*, 1989, 3513; (*e*) P. H. Rieger, in *Organometallic Radical Processes*, ed. W. C. Trogler, Elsevier, Amsterdam, 1990; (*f*) G. A. Carriedo, N. G. Connelly, E. Perez-Carreno, A. G. Orpen, A. L. Rieger, P. H. Rieger, V. Riera and G. M. Rosair, *J. Chem. Soc., Dalton Trans.*, 1993, 3103.
9 C. G. Krespan, *J. Am. Chem. Soc.*, 1961, **83**, 3434.
10 C. H. Langford, E. Billig, S. I. Shupack and H. B. Gray, *J. Am. Chem. Soc.*, 1967, **86**, 2958.
11 G. M. Sheldrick, SHELXTL 5.1, Siemens Analytical X-Ray Instruments Inc., Madison, WI.
12 G. M. Sheldrick, *J. Appl. Crystallogr.*, in the press.
13 A. J. Stone, *Proc. Roy. Soc. London, Ser. A*, 1963, **271**, 424.
14 J. R. Morton and K. F. Preston, *J. Magn. Reson.*, 1978, **30**, 577.
15 F. H. Allen, O. Kennard, D. G. Watson, L. Brammer, A. G. Orgen and R. Taylor, *J. Chem. Soc., Perkin Trans. 2*, 1987, S1.
16 D. Sellmann, M. Geck, F. Knoch, G. Ritter and J. Dengler, *J. Am. Chem. Soc.*, 1991, **113**, 3819.
17 Computer-aided Chemistry program, Version 3.5, CAChe Scientific Inc., Beaverton, OR, 1992.

Received 1*st June* 1994; *Paper* 4/03253E